Letters

Reference-Feedforward Power-Synchronization Control

Lennart Harnefors, *Fellow, IEEE*, F. M. Mahafugur Rahman, Marko Hinkkanen, *Senior Member, IEEE*, and Mikko Routimo, *Member, IEEE*

***Abstract*—In this letter, an enhancement of power-synchronization control is proposed, whereby pole–zero cancellation in the closed-loop system is achieved. An effect thereof is that step-response ringing and overshoot are eliminated. For strong grids, the closed-loop bandwidth increases, allowing a shorter step-response rise time.**

***Index Terms*—Grid-connected converters, robustness, stability analysis, voltage-source converters (VSCs).**

I. Introduction

POWER-SYNCHRONIZATION control (PSC) [1] is based on emulating the dynamics of a synchronous machine by a grid-connected voltage-source converter (VSC). The scheme was originally conceived to allow a stable interconnection with a very weak grid [2]. Its properties have been studied in detail over the years. Two recent examples are the large-signal transient stability analysis presented in [3] and the analytic selection of the power-control gain derived in [4]. In addition, in [4], an empirical selection recommendation for the so-called active resistance (which resembles the proportional gain of a current controller) is given. A robust design, with guaranteed stability margins of the power control loop, is obtained irrespective of the grid strength.

The great majority of papers on PSC consider weak-grid connections and/or grid-forming control, e.g., [5]–[8]. For robustness it is desirable that PSC should perform well also in a strong-grid connection. Unfortunately, even with the robust design in [4], the performance of PSC is inferior to that of traditional vector current control with cascaded outer loops. The closed-loop bandwidth is inherently limited and typically the step response exhibits overshoot and/or ringing.

This shortcoming is here rectified by the enhancement reference-feedforward PSC (RFPSC). In addition to using the power reference in the power control law, it is fed forward to the active-resistance part [9]. It is shown that this places the zeros of the closed-loop system so that they (near-exactly) cancel a complex pole pair, reducing the system order from three to one. The pole–zero cancellation occurs irrespective of the grid inductance, thus ensuring robustness.

Design and analysis of RFPSC are presented in Section II, followed by experimental verification in Section III.

Manuscript received December 3, 2019; revised January 3, 2020; accepted January 19, 2020. Date of publication February 3, 2020; date of current version May 1, 2020. This work was supported by ABB. *(Corresponding author: Lennart Harnefors.)*

L. Harnefors is with the ABB, Corporate Research, 722 26 Västerås, Sweden (e-mail: lennart.harnefors@se.abb.com).

F. M. M. Rahman and M. Hinkkanen are with the Department of Electrical Engineering and Automation, Aalto University, 02150 Espoo, Finland (e-mail: f.rahman@aalto.fi; marko.hinkkanen@aalto.fi).

M. Routimo is with the ABB Oy Drives, 00380 Helsinki, Finland (e-mail: mikko.routimo@fi.abb.com).

Color versions of one or more of the figures in this letter are available online at https://ieeexplore.ieee.org.

Digital Object Identifier 10.1109/TPEL.2020.2970991

II. Theoretical Results

A. Design

In PSC, the converter voltage, expressed in the stationary $\alpha\beta$ frame, is given as

$$\mathbf{v}^s = \mathbf{v}e^{j\theta} \tag{1}$$

assuming operation in the linear pulsewidth-modulation region, controller latency neglected, and switching harmonics disregarded. With current and power direction out of the converter, angle θ—which defines the synchronously rotating dq frame—is governed by the (active) power control law

$$\frac{d\theta}{dt} = \omega_1 + K_p(P_{\mathrm{ref}} - P) \tag{2}$$

where ω_1 is the fundamental angular frequency, K_p is the power-control gain, and P_{ref} is the power reference

$$P = \kappa \mathrm{Re}\{\mathbf{v}^s(\mathbf{i}^s)^*\} = \kappa \mathrm{Re}\{\mathbf{v}\mathbf{i}^*\}, \qquad \kappa = \frac{3}{2}K^2 \tag{3}$$

is the active output power, and K is the space-vector scaling constant. For per-unit (p.u.) normalization of the quantities or power-invariant vector scaling ($K = \sqrt{3/2}$), $\kappa = 1$. Moreover, PSC gives the dq-frame converter voltage as

$$\mathbf{v} = V + R_a(\mathbf{i}_{\mathrm{ref}} - \mathbf{i}) \tag{4}$$

where V is considered constant (nominally 1 p.u.), although in practice it may be varied via a closed control loop for the point-of-common-coupling voltage or the reactive power [1], [10]. The second term is that of the active resistance R_a, expressed as a proportional control law. In conventional PSC, $\mathbf{i}_{\mathrm{ref}}$ is selected as a filtering of the converter current $\mathbf{i} = i_d + ji_q$ by the low-pass filter $H(s) = \omega_b/(s + \omega_b)$ [4].

In the steady state, $\mathbf{i}_{\mathrm{ref}} - \mathbf{i} = 0$, simplifying (3) to $P = \kappa V i_d$. This motivates selecting the d component of $\mathbf{i}_{\mathrm{ref}}$ as $P_{\mathrm{ref}}/(\kappa V)$, whereas the low-pass filtering for the q component remains, i.e.

$$\mathbf{i}_{\mathrm{ref}} = \frac{P_{\mathrm{ref}}}{\kappa V} + jH(s)\mathrm{Im}\{\mathbf{i}\} \tag{5}$$

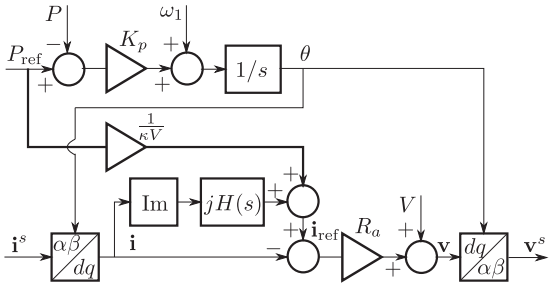

Fig. 1. Block diagram of RFPSC. The thick line shows the feedforward path for the power reference.

which constitutes the invention in RFPSC [9]. The block diagram shown in Fig. 1 is obtained.

Remark: Being a voltage-stiff control scheme, PSC gives injection of negative-sequence current as response to an unbalanced grid. The d component of $\mathbf{i}_{\rm ref}$ has low negative-sequence content; for conventional PSC because of filtering and for RFPSC due to its selection as a quotient of two references. Hence, the two PSC variants have virtually identical unbalanced-grid responses.

B. Analysis

The closed-loop system from $P_{\rm ref}$ to P resulting from RFPSC is analyzed here. In accordance with [1] and [4], a purely inductive grid impedance, with inductance L, behind an infinite bus with the stiff voltage V_g is assumed. Consequently,

$$\mathbf{v}^s - sL\mathbf{i}^s = \mathbf{v}_g^s = V_g e^{j\omega_1 t} \tag{6}$$

where $s = d/dt$. Since the coordinate transformation in (1) and the active-power expression in (3) both are nonlinear, small-signal analysis is required. Identically to [4], the involved variables are expressed as perturbations (denoted by the prefix Δ) about operating points as follows:

$$\theta = \omega_1 t + \theta_0 + \Delta\theta \qquad \mathbf{i} = \mathbf{i}_0 + \Delta\mathbf{i} \tag{7}$$

where $\mathbf{i}_0 = i_{d0} + ji_{q0}$. With (7), (6) is transformed to the dq frame as follows:

$$\mathbf{v} - [s + j\underbrace{(\omega_1 + \dot{\Delta\theta})}_{\dot\theta}]L\mathbf{i} = V_g e^{-j(\theta_0+\Delta\theta)}. \tag{8}$$

For the conventional PSC selection $\mathbf{i}_{\rm ref} = H(s)\mathbf{i}$, the small-signal form of (4) becomes $\Delta\mathbf{v} = R_a[H(s)-1]\Delta\mathbf{i}$, whereas the RFPSC selection in (5) yields $\Delta\mathbf{v} = R_a[\Delta P_{\rm ref}/(\kappa V) + jH(s){\rm Im}\{\Delta\mathbf{i}\} - \Delta\mathbf{i}]$. The bandwidth of $H(s)$ is selected low, typically $\omega_b = 0.1$ p.u. [4]. This allows approximating $H(s) = 0$ without significantly impairing the accuracy of the results, yielding the following perturbation form of (4):

$$\Delta\mathbf{v} = R_a\left(\xi\frac{\Delta P_{\rm ref}}{\kappa V} - \Delta\mathbf{i}\right), \qquad \xi = \begin{cases} 0 \text{ for conv. PSC} \\ 1 \text{ for RFPSC.} \end{cases} \tag{9}$$

Straightforward comparison of the two variants, conventional PSC and RFPSC, is thereby permitted. Substituting (9) in (8), approximating $e^{-j\Delta\theta} \approx 1 - j\Delta\theta$, and neglecting cross terms between perturbation variables yields

$$[R_a + (s+j\omega_1)L]\Delta\mathbf{i} = \frac{\xi R_a}{\kappa V}\Delta P_{\rm ref} + j(V_g e^{-j\theta_0} - sL\mathbf{i}_0)\Delta\theta + V - j\omega_1 L\mathbf{i}_0 - V_g e^{-j\theta_0} \tag{10}$$

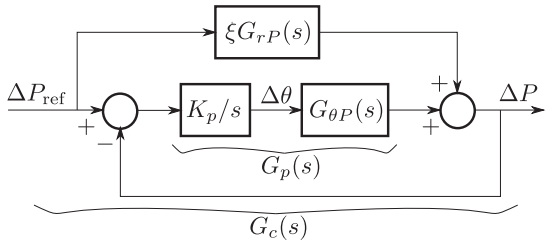

Fig. 2. Linearized closed-loop system, where RFPSC is obtained for $\xi = 1$.

where the last three terms on the right-hand side must sum up to zero, giving $V_g e^{-j\theta_0} = V - j\omega_1 L\mathbf{i}_0$. Solving for $\Delta\mathbf{i}$ yields the following relation:

$$\Delta\mathbf{i} = \underbrace{\frac{j[V-(s+j\omega_1)L\mathbf{i}_0]}{R_a+(s+j\omega_1)L}}_{\mathbf{G}_{\theta i}(s)}\Delta\theta + \underbrace{\frac{\frac{\xi R_a}{\kappa V}}{R_a+(s+j\omega_1)L}}_{\mathbf{G}_{ri}(s)}\Delta P_{\rm ref}. \tag{11}$$

Introduction of perturbation variables in (3) gives, after linearization

$$\Delta P = \kappa{\rm Re}\{V\Delta\mathbf{i}^* + \mathbf{i}_0^*\Delta\mathbf{v}\}. \tag{12}$$

Substitution of (9) in (12) yields

$$\Delta P = \kappa{\rm Re}\{V\Delta\mathbf{i}^* - R_a\mathbf{i}_0^*\Delta\mathbf{i}\} + \frac{\xi R_a i_{d0}}{V}\Delta P_{\rm ref} \tag{13}$$

in which (11) is substituted, giving

$$\Delta P = \underbrace{\kappa{\rm Re}\{V\mathbf{G}_{\theta i}^*(s) - R_a\mathbf{i}_0^*\mathbf{G}_{\theta i}(s)\}}_{G_{\theta P}(s)}\Delta\theta + \underbrace{\xi\left[\frac{R_a i_{d0}}{V} + \frac{\kappa}{\xi}{\rm Re}\{V\mathbf{G}_{ri}^*(s) - R_a\mathbf{i}_0^*\mathbf{G}_{ri}(s)\}\right]}_{G_{rP}(s)} \times \quad \Delta P_{\rm ref}. \tag{14}$$

The real part is evaluated for s real, resulting in

$$G_{\theta P}(s) = \frac{\kappa V^2}{\omega_1 L}\frac{as^2 + (1+a+b)\omega_1^2}{s^2 + 2\alpha s + \omega_1^2 + \alpha^2} \tag{15}$$

$$G_{rP}(s) = \frac{cs^2 + \alpha(1+c)s + (c+d)\omega_1^2 + \alpha^2}{s^2 + 2\alpha s + \omega_1^2 + \alpha^2} \tag{16}$$

where

$$\alpha = \frac{R_a}{L} \qquad a = \frac{\omega_1 L i_{q0}}{V} \qquad b = -\frac{R_a^2}{V}\left(\frac{i_{q0}}{\omega_1 L} + \frac{|\mathbf{i}_0|^2}{V}\right)$$
$$c = \frac{R_a i_{d0}}{V} \qquad d = \frac{R_a^2 i_{q0}}{\omega_1 L V}. \tag{17}$$

Combining (14) with the power control law (2), expressed in perturbation variables as $\Delta\theta = (K_p/s)(\Delta P_{\rm ref} - \Delta P)$, the closed-loop system, shown in Fig. 2, is obtained. As $G_p(s)$ is invariant of ξ, RFPSC does not affect the feedback loop in Fig. 2, and consequently not the poles of the closed-loop system $G_c(s)$. This motivates adopting the gain selection in [4]

$$K_p = \frac{\omega_1 R_a}{\kappa V^2} \tag{18}$$

which gives ample stability margins.

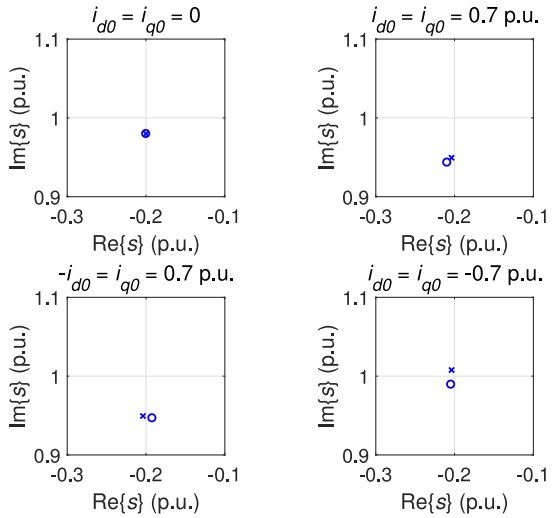

Fig. 3. Pole–zero plots for $V = \omega_1 = 1$ p.u., $L = 0.5$ p.u., $R_a = 0.2$ p.u., and various operating points $\mathbf{i}_0 = i_{d0} + ji_{q0}$. Exact pole–zero cancellation is obtained for $\mathbf{i}_0 = 0$, near-exact otherwise.

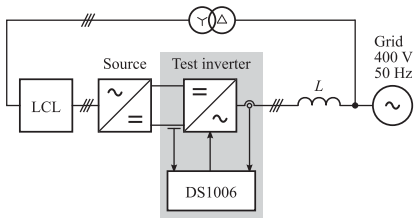

Fig. 4. Schematic of the experimental setup.

TABLE I
TEST-SYSTEM DATA

Variable/parameter	Actual value	Normalized value
Rated power	12.7 kVA	1 p.u.
Rated voltage	$\sqrt{2/3} \cdot 400$ V	1 p.u.
Rated current	$\sqrt{2} \cdot 18.3$ A	1 p.u.
Base impedance	12.6 Ω	1 p.u.
Fundamental frequency	50 Hz	1 p.u.
Sampling frequency	8 kHz	160 p.u.
Switching frequency	4 kHz	80 p.u.
Active resistance R_a	4.4 Ω	0.2 p.u.
Filter bandwidth ω_b	31 rad/s	0.1 p.u.

Block-diagram reductions in Fig. 2 give $G_c(s) = [G_p(s) + \xi G_{rP}(s)]/[1 + G_p(s)]$. Substituting (15) and (16) in this relation yields

$$G_c(s) = \frac{\xi c s^3 + k_2 s^2 + k_1 s + (1+a+b)\alpha\omega_1^2}{s^3 + (2+a)\alpha s^2 + (\alpha^2 + \omega_1^2)s + (1+a+b)\alpha\omega_1^2} \tag{19}$$

where $k_2 = [a + \xi(1+c)]\alpha$ and $k_1 = \xi[(c+d)\omega_1^2 + \alpha^2]$. The denominator can be approximately factorized as $[s + (1 + a + b)\alpha](s^2 + \alpha s + \omega_1^2)$, expanding to $s^3 + (2 + a + b)\alpha s^2 + [(1 + a + b)\alpha^2 + \omega_1^2]s + (1 + a + b)\alpha\omega_1^2$. The coefficients for s^2 and s are, thus, imperfectly matched. An approximate factorization of the numerator is, for $\xi = 1$, given as $[cs + (1 + a + b)\alpha](s^2 + \alpha s + \omega_1^2)$. Expansion shows that the coefficients for s^2 and s are imperfect matches here as well. However, all

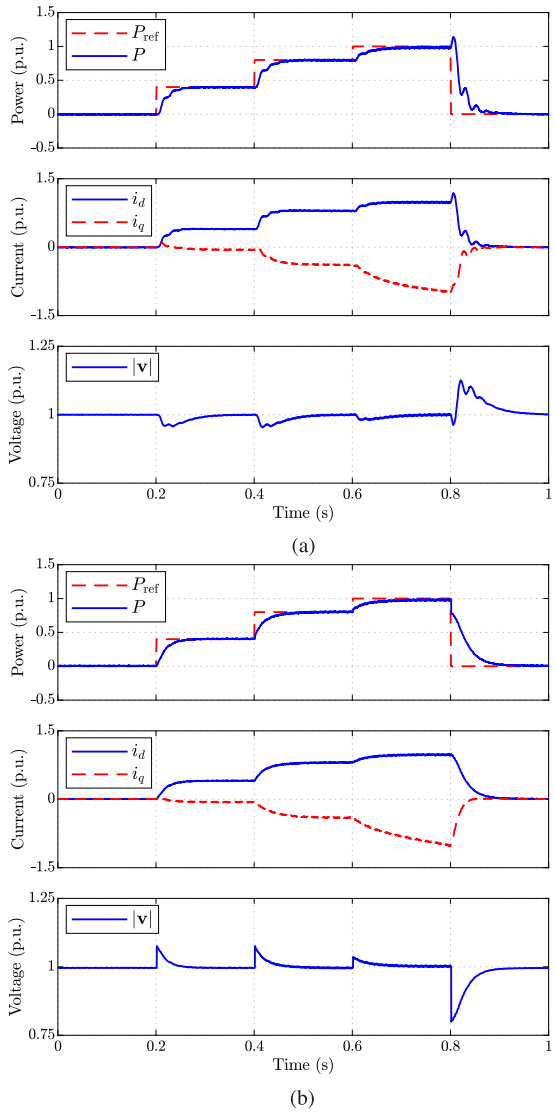

Fig. 5. Step responses for a weak grid, $L = 1$ p.u. (a) Conventional PSC. (b) RFPSC.

mismatches are small for $\{|a|, |b|, |c|\} \ll 1$. This is normally the case, as long as R_a is moderate; $R_a = 0.2$ p.u. is suggested in [4]. By the approximate factorizations, the second-degree factors cancel, reducing (19) to the first-order system

$$G_c(s) \approx \frac{cs + (1+a+b)\alpha}{s + (1+a+b)\alpha}. \tag{20}$$

RFPSC (i.e., $\xi = 1$) with the gain selection in (18) is required for this pole–zero cancellation to occur. For $\mathbf{i}_0 = 0 \Rightarrow a = b = c = 0$, the polynomial factorizations are exact, and, thus, also the pole–zero cancellation. For other operating points $\mathbf{i}_0$, yet a near-exact cancellation is obtained, as exemplified in Fig. 3.

As found in [4], the cancelled pole pair is dominant for strong grids (i.e., small L), effectively limiting the closed-loop bandwidth to $\omega_1 = 1$ p.u. for conventional PSC. On the contrary, for RFPSC, the remaining pole of (20) gives the closed-loop bandwidth $(1 + a + b)\alpha$, which for a strong grid easily exceeds 1 p.u. For example, $L = 0.1$ p.u., $R_a = 0.2$ p.u., and $\mathbf{i}_0 = 0$ give $(1 + a + b)\alpha = \alpha = 2$ p.u. In addition, since the pole pair

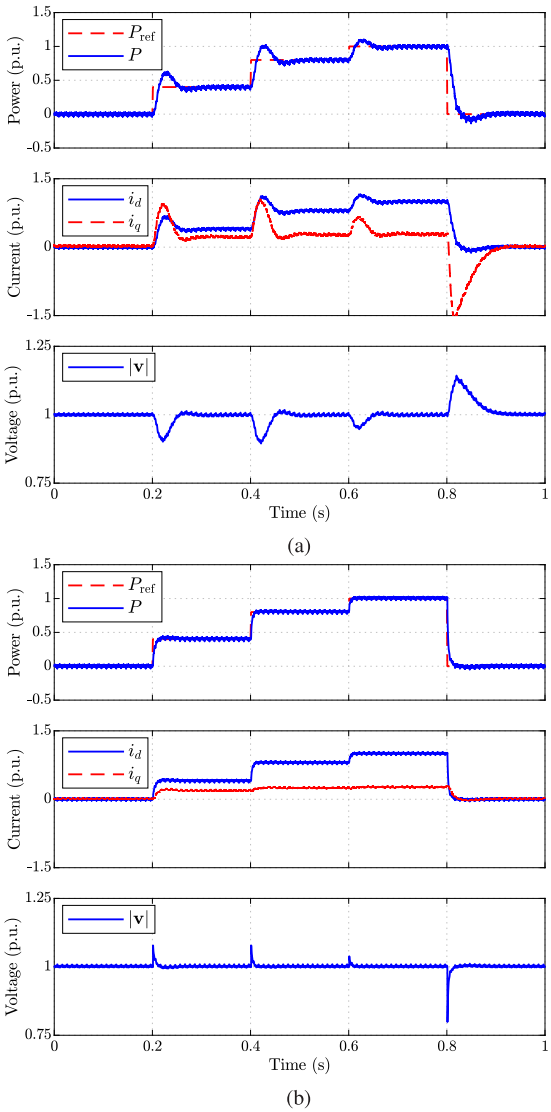

Fig. 6. Step responses for a strong grid, $L = 0.1$ p.u. (a) Conventional PSC. (b) RFPSC.

is located fairly close to the imaginary axis (see Fig. 3), its cancellation generally improves damping.

III. Experimental Results

RFPSC is here experimentally compared with conventional PSC, using the same back-to-back (grid and dc source) two-level VSC system as in [4]—see the schematic depicted in Fig. 4—whose data are given in Table I. Control is implemented on a dSPACE DS1006 processor board. The dc link is controlled from the dc source.

Figs. 5 and 6 show results for four successive steps in P_{ref}, respectively, for a weak and a strong grid, with conventional PSC as well as with RFPSC. (The subfigures for conventional PSC are repeated from [4], for clarity.) The following can be observed.

1) The step-response rise times in the weak-grid case are similar for conventional PSC and RFPSC. This was to be expected, since, for a weak grid, the real pole of the closed-loop system is dominant. Cancellation of the complex pole pair only gives a slight increase of the closed-loop bandwidth. On the other hand, the tendency to ringing in the step response is eliminated.
2) In the strong-grid case, RFPSC gives shorter rise times than conventional PSC and, perhaps even more importantly, eliminates the overshoots. In addition, the voltage-magnitude transients are significantly reduced.
3) In accordance with the model in (20) resulting from the pole–zero cancellation, all step responses for RFPSC resemble first-order exponentials.

IV. Conclusion

In this letter, the enhancement RFPSC of conventional PSC was presented. It involves feeding the power reference forward to the active-resistance part of the control law. When observing the robustifying gain selection in (18), the complex pole pair of the closed-loop system is (near-exactly) cancelled. Compared with conventional PSC, this was shown to eliminate step-response ringing for weak grids. For strong grids, a shorter step-response rise time is obtained and overshoot is avoided, allowing performance similar to that of vector current control. The design was shown to be robust in the sense that, irrespective of the grid inductance L, the step response resembles a first-order exponential whose rise time is proportional to L. Knowledge of L is not required for the robust design, as fundamentally shown by the gain selection given in (18). A suitable topic for further research is performance analysis for a generic grid impedance.

References

[1] L. Zhang, L. Harnefors, and H.-P. Nee, "Power-synchronization control of grid-connected voltage-source converters," *IEEE Trans. Power Syst.*, vol. 25, no. 2, pp. 809–920, May 2010.
[2] L. Zhang, L. Harnefors, and H.-P. Nee, "Interconnection of two very weak ac systems by VSC-HVDC links using power-synchronization control," *IEEE Trans. Power Syst.*, vol. 26, no. 1, pp. 344–355, Feb. 2011.
[3] H. Wu and X. Wang, "Design-oriented transient stability analysis of grid-connected converters with power synchronization control," *IEEE Trans. Ind. Electron.*, vol. 66, no. 8, pp. 6473–6482, Aug. 2019.
[4] L. Harnefors, M. Hinkkanen, U. Riaz, F. M. M. Rahman, and L. Zhang, "Robust analytic design of power-synchronization control," *IEEE Trans. Ind. Electron.*, vol. 66, no. 8, pp. 5810–5819, Aug. 2019.
[5] K. M. Alawasa and Y. A. R. I. Mohamed, "Impedance and damping characteristics of grid-connected VSCs with power synchronization control," *IEEE Trans. Power Syst.*, vol. 30, no. 2, pp. 952–961, Mar. 2015.
[6] A. A. A. Radwan and Y. A. R. I. Mohamed, "Power synchronization control for grid-connected current-source inverter-based photovoltaic systems," *IEEE Trans. Energy Convers.*, vol. 31, no. 3, pp. 1023–1036, Sep. 2016.
[7] S. I. Nanou and S. A. Papathanassiou, "Grid code compatibility of VSC-HVDC connected offshore wind turbines employing power synchronization control," *IEEE Trans. Power Syst.*, vol. 31, no. 6, pp. 5042–5050, Nov. 2016.
[8] S. I. Nanou and S. A. Papathanassiou, "Frequency control of island VSC-HVDC links operating in parallel with ac interconnectors and on-site generation," *IEEE Trans. Power Del.*, vol. 33, no. 1, pp. 447–454, Feb. 2018.
[9] L. Harnefors and L. Zhang, "Method and control system for controlling a voltage source converter using power-synchronization control," U.S. Patent 10 389 129 B2, Aug. 2019.
[10] H. Wu *et al.*, "Small-signal modeling and parameters design for virtual synchronous generators," *IEEE Trans. Ind. Electron.*, vol. 64, no. 7, pp. 4292–4303, Jul. 2016.